Int J Thermophys (2017) 38:7
DOI 10.1007/s10765-016-2143-0

ICPPP 18

Study of Exciton Hopping Transport in PbS Colloidal Quantum Dot Thin Films Using Frequency- and Temperature-Scanned Photocarrier Radiometry

Lilei Hu[1] · Andreas Mandelis[1,2] · Alexander Melnikov[1] · Xinzheng Lan[2] · Sjoerd Hoogland[2] · Edward H. Sargent[2]

Received: 10 October 2015 / Accepted: 15 October 2016 / Published online: 7 November 2016

Abstract Solution-processed colloidal quantum dots (CQDs) are promising materials for realizing low-cost, large-area, and flexible photovoltaic devices. The study of charge carrier transport in quantum dot solids is essential for understanding energy conversion mechanisms. Recently, solution-processed two-layer oleic-acid-capped PbS CQD solar cells with one layer treated with tetrabutylammonium iodide (TBAI) serving as the main light-absorbing layer and the other treated with 1,2-ethanedithiol (EDT) acting as an electron-blocking/hole-extraction layer were reported. These solar cells demonstrated a significant improvement in power conversion efficiency of 8.55% and long-term air stability. Coupled with photocarrier radiometry measurements, this work used a new trap-state mediated exciton hopping transport model, specifically for CQD thin films, to unveil and quantify exciton transport mechanisms through the extraction of hopping transport parameters including exciton lifetimes, hopping diffusivity, exciton detrapping time, and trap-state density. It is shown that PbS-TBAI has higher trap-state density than PbS-EDT that results in higher PbS-EDT exciton lifetimes. Hopping diffusivities of both CQD thin film types show similar temperature dependence, particularly higher temperatures yield higher hopping diffusivity. The higher diffusivity of PbS-TBAI compared with PbS-EDT indicates that PbS-TBAI is a much better photovoltaic material than PbS-EDT. Furthermore, PCR tempera-

This article is part of the selected papers presented at the 18th International Conference on Photoacoustic and Photothermal Phenomena.

✉ Andreas Mandelis
mandelis@mie.utoronto.ca

1 Center for Advanced Diffusion-Wave and Photoacoustic Technologies (CADIPT), Department of Mechanical and Industrial Engineering, University of Toronto, Toronto, ON M5S 3G8, Canada

2 Edward S. Rogers Sr. Department of Electrical and Computer Engineering, University of Toronto, Toronto, ON M5S 3G4, Canada

ture spectra and deep-level photothermal spectroscopy provided additional insights to CQD surface trap states: PbS-TBAI thin films exhibit a single dominant trap level, while PbS-EDT films with lower trap-state densities show multiple trap levels.

Keywords CQD solar cells · Detrapping lifetime · Exciton lifetimes · Hopping transport · Hopping diffusivity · Lead sulfide (PbS)colloidal quantum dot · Photocarrier radiometry (PCR) · Trap states

1 Introduction

Solution-processed colloidal quantum dots with tunable bandgaps through dot size control have become promising candidates for low-cost, large-area, flexible, and lightweight photovoltaic devices over the last few decades [1–3]. QD surface ligands and photovoltaic device architectures play crucial roles in solar cell energy conversion efficiency. Chuang et al. [2,3] demonstrated newly structured solar cells with high power efficiency of 8.55% and a long-term air stability through engineering PbS-TBAI and PbS-EDT CQD thin films that served as the main light-absorbing layer and electron-blocking/hole-extraction layer, respectively. However, CQD solar cell efficiency is still significantly limited by surface trap states of CQDs, while the mechanisms behind are still not well understood.

Photocarrier radiometry (PCR) is a dynamic spectrally gated frequency-domain photoluminescence (PL) modality that is able to yield quantitative information about exciton transport dynamics with accuracy and precision superior to time-resolved PL due to its intrinsically high signal-to-noise ratio (SNR), which is based on narrowband lock-in demodulation [4,5]. Coupled with PCR frequency scans, an exciton hopping transport model for CQDs was used to reveal photocarrier transport dynamics in CQD thin films and extracted several transport parameters: exciton lifetimes, trap state density, hopping diffusivity, and detrapping lifetimes. Furthermore, PCR thermal spectra (temperature scans) was measured and showed evidence of CQD trap states and temperature-dependent capture and emission processes [6].

2 Exciton Hopping Transport Theory

When PbS CQDs are excited optically, the rate equation for exciton population $N_i\,(x,t)$ in quantum dot i must include the presence of trap states, acting as thermal emission sources and capture canters. The rate equation for exciton population in the i_{th} QD with the presence of bulk or surface trap states can be expressed as an extension of the exciton relaxation model as proposed in Ref. [7] by adding additional trap-state emission and capture kinetics:

$$\frac{\partial N_i\,(x,t)}{\partial t} = -\frac{\partial J_e\,(x,t)}{\partial x} + e_i\,(T)\,n_T\,(x,t) - C_i N_i\,(x,t)\,[N_T - n_T\,(x,t)] - \frac{N_i\,(x,t)}{\tau} + G_0\,(x,t) \tag{1}$$

N_i and e_i are exciton population and thermal emission rate, respectively. In addition, n_T, N_T, G_0, and C_i represent trapped exciton density, trap-state density, exciton generation rate, and the exciton capture coefficient, respectively; exciton current $J_e(x,t) = -D_h(T)\frac{\partial N_i(x,t)}{\partial x}$, where $D_h(T) = \frac{L^2}{\tau_0}e^{-\gamma L - E_a/kT}$, in which E_a is the hopping transport activation energy, $D_h(T)$ is the hopping diffusivity, L is the interdot distance, γ is the exciton hopping probability, τ_0 is the characteristic hopping time, T is the absolute temperature, and k is the Boltzmann constant . L is varied by exchange ligands. The kinetic equation for the trapped exciton population, $n_T(x,t)$, is

$$\frac{\partial n_T(x,t)}{\partial t} = -e_i(T)\,n_T(x,t) + C_i N_i(x,t)\,[N_T - n_T(x,t)] \tag{2}$$

Using a two-level (singlet-triplet state splitting) colloidal quantum dot energy model with exciton populations N_s and N_t in singlet and triplet states, respectively, as well as an energy difference of ΔE between these two levels, the rate equation for the total exciton density, $N_i(x,t)$, in quantum dot (i) is given by

$$\begin{aligned}\frac{\partial N_i(x,t)}{\partial t} &= \frac{\partial N_s(x,t)}{\partial t} + \frac{\partial N_t(x,t)}{\partial t} = \left(1 + R_{st}e^{-\frac{\Delta E}{kT}}\right)\frac{\partial N_t(x,t)}{\partial t}\\ &= [1 + A(T)]\,\frac{\partial N_t(x,t)}{\partial t},\end{aligned} \tag{3}$$

where $N_i = N_s + N_t$, and $A(T) = R_{st}e^{-\Delta E/kT}$ which is the transition rate for exciton transfer between singlet and triplet states, and the degeneracy ratio R_{st} between singlet-triplet states is equal to $\frac{1}{3}$ [7]. In case of modulated optical excitation of CQDs, the exciton density wave (modulated population) of the triplet exciton states $n_t(x,\omega)$ can be expressed as:

$$\begin{aligned}&\frac{d^2 n_t(x,\omega)}{\mathrm{d}x^2} - \frac{1}{D_h(T)}\left[i\omega + \frac{1}{\tau_E(T)} - \frac{C_i N_T}{[1 + A(T)]\,[1 + i\omega\tau_i(T)]}\right] n_t(x,\omega)\\ &= -\frac{G_0\beta e^{-\beta x}}{D_h(T)\,[1 + A(T)]}\end{aligned} \tag{4}$$

Here, τ_E is the effective exciton lifetime, defined by $\frac{1}{\tau_E(T)} = \frac{1}{\tau_2(T)} + C_i N_T$ ($\frac{1}{\tau_2(T)}$ is the total exciton decay rate, equal to the sum of radiative and non-radiative rates, i.e., $\tau_2(T)$ is the total exciton lifetime), and $\tau_i(T)$ is the detrapping (thermal emission) lifetime as defined to be $\frac{1}{\tau_i(T)} \equiv e_i(T)$. β is the quantum dot layer optical absorption coefficient. For simplification, we assigned the complex exciton density-wavenumber to be

$$K_1^2(T;\omega) \equiv \frac{1}{D_h(T)}\left\{i\omega + \frac{1}{\tau_E(T)} - \frac{C_i N_T}{[1 + A(T)]\,[1 + i\omega\tau_i(T)]}\right\}, \tag{5}$$

and the quantity

$$K_2(T,\beta) \equiv \frac{G_0\beta}{D_h(T)\,[1 + A(T)]}. \tag{6}$$

Equation 4 was solved by applying quenching boundary conditions to CQD thin films with a thickness of d, i.e., $n_t(x,\omega) = 0$, at $x = 0$ and d [8]. The mathematical expression of PCR signal can be obtained from Ref. [4]

$$S(\omega) = F(\lambda_1, \lambda_2) \int_0^d n_i(x,\omega)\,\mathrm{d}x \tag{7}$$

where $F(\lambda_1, \lambda_2)$ is an instrumental coefficient, dependent on the spectral bandwidth of the photodetector. Finally, the PCR signal as a function of exciton transport parameters and trap-state density is given by:

$$\frac{S(\omega)}{F(\lambda_1,\lambda_2)} = \left[\frac{K_2(T,\beta)}{\beta^2 - K_1^2(T,\omega)}\right]\left\{\frac{\left(1+e^{-\beta d}\right)\left(1-e^{-K_1 d}\right)^2}{K_1\left(1-e^{-2K_1 d}\right)} - \frac{1}{\beta}\left(1-e^{-\beta d}\right)\right\} \tag{8}$$

3 Experimental Materials and System

Two iodide-passivated PbS CQD thin films were spin-coated onto glass substrates and then separately treated with ligands TBAI and EDT for the purpose of solid-state ligand treatments as described in Ref. [9,10]. The thickness of both CQD thin films is 200 nm as measured using scanning electron microscopy (SEM). Transmission electron microscopy (TEM) and atomic force microscopy (AFM) were used to characterize these nanolayers. It was found that these CQDs, same as those reported earlier [9, 10], exhibited spheroidal shape with a mean diameter of 3 nm. In addition, TEM demonstrated the interdot distances of PbS-EDT and PbS-TBAI were in a range of 2 nm–5 nm [11–13]. As shown in Fig. 1a, the PCR experimental setup is the same as that used by Wang et al. [7], accompanied by an 830 nm laser, sine-wave modulated from 10 Hz to100 kHz with a function generator. Furthermore, a 1 μm long-pass filter was placed in front of the InGaAs photodetector to block excitation beams, and no short-pass filter was applied due to the negligible thermal infrared contributions to the PCR signal. Temperature control was carried out by using a Linkam LTS350 cryogenic chamber that allowed a maintenance of constant temperatures in a range between 77 K and 520 K.

4 Results and Discussion

Figure 1b–e show the PCR amplitude and phase frequency scans of PbS-TBAI/EDT and the best-fit to each curve using Eq. 8. With decreasing temperature, the increased high-frequency PCR phase lags are observed, which are due to the enhanced exciton de-excitation lifetimes, and the higher PCR amplitudes are caused by reduced non-radiative recombination probability scaling with phonon population [7]. For theoretical fitting, Eq. 8 was recast into amplitude and phase channels $A(\omega) = \sqrt{F_\mathrm{R}^2(\omega) + F_\mathrm{I}^2(\omega)}$ and $\varphi(\omega) = \tan^{-1}\left[\frac{F_\mathrm{I}(\omega)}{F_\mathrm{R}(\omega)}\right]$, respectively. $F_\mathrm{I}(\omega)$ and $F_\mathrm{R}(\omega)$ are the imaginary and

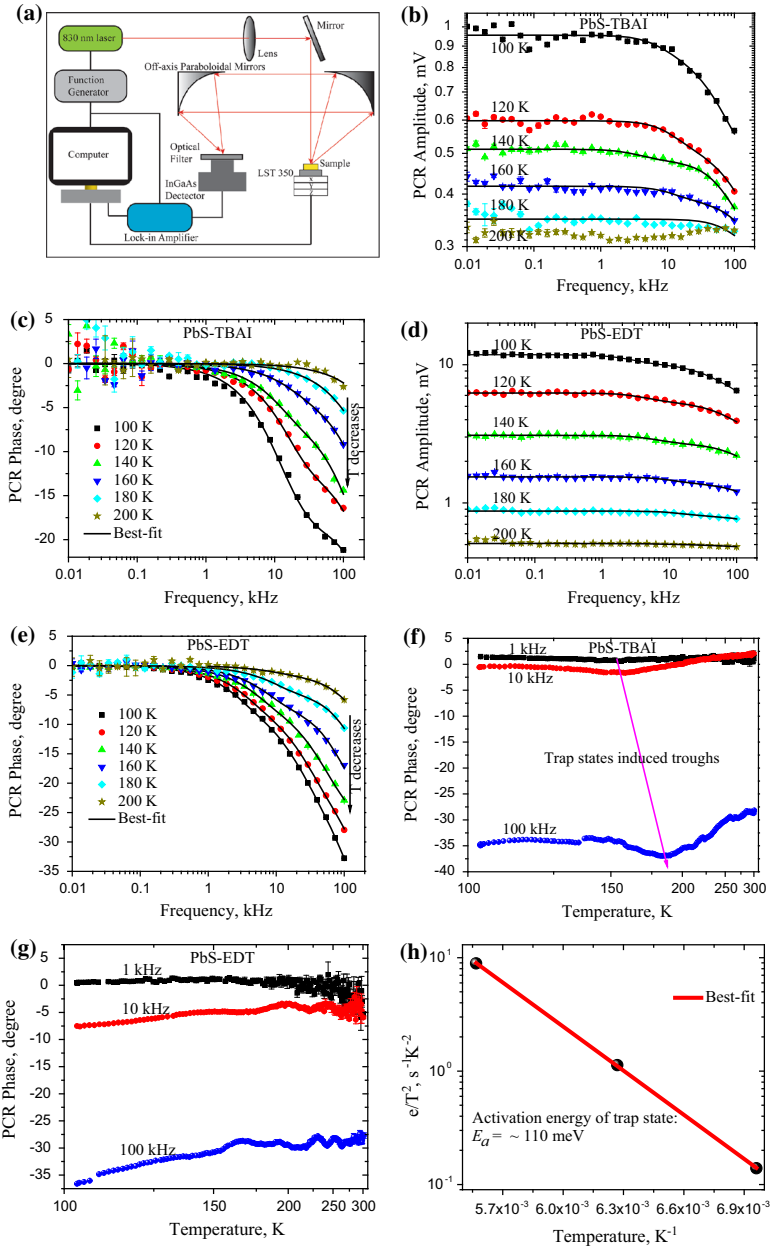

Fig. 1 (a) Schematic diagram of the photocarrier radiometry (PCR) setup for CQD frequency- and temperature-scan. (b)–(e) frequency-scanned PCR amplitude and phase of PbS-TBAI and PbS-EDT colloidal quantum dot (CQD) thin films at low temperatures (100–200 K), and best-fits to each curve to Eq. 8. (f, g) PCR phases from temperature scans of PbS-TBAI and PbS-EDT, respectively. For PbS-TBAI, the trap-state induced trough moves to higher temperatures with increasing laser modulation frequency indicating a single dominant trap level. In contrast, PbS-EDT with lower trap-state density shows a multiple-trough feature. (h) Arrhenius plot of the PCR phase troughs shown in Fig.1f and best-fits to Eq. 9

Table 1 Summary of parameters measured from the PCR frequency-scan phase channel

Temperature	D_h (cm^2 /s)		τ_2 (μs)		τ_i (μs)		N_T (cm^{-3})		τ_E (μs)	
(K)	PbS-TBAI	PbS-EDT	PbS-TBAI	PbS-EDT	PbS-TBAI	PbS-EDT	PbS-TBAI	PbS-EDT	PbS-TBAI	PbS-EDT
100	5.29×10^{-5}	3.23×10^{-5}	3.86	10.20	3.01	24.60	4.04×10^{17}	9.30×10^{16}	1.94	7.74
	$\pm 6.03 \times 10^{-6}$	$\pm 1.33 \times 10^{-5}$	±0.044	±0.037	±0.17	±0.11	$\pm 2.80 \times 10^{17}$	$\pm 3.93 \times 10^{16}$	±0.37	±0.012
120	2.14×10^{-4}	6.76×10^{-5}	2.35	7.31	3.22	17.30	4.46×10^{17}	1.78×10^{17}	1.30	5.52
	$\pm 4.31 \times 10^{-5}$	$\pm 1.20 \times 10^{-5}$	±0.014	±0.019	±0.034	±0.16	$\pm 1.47 \times 10^{17}$	$\pm 6.83 \times 10^{16}$	±0.008	±0.007
140	2.30×10^{-4}	1.50×10^{-4}	1.71	4.47	5.52	12.00	3.41×10^{17}	1.24×10^{17}	1.09	3.34
	$\pm 3.06 \times 10^{-5}$	$\pm 3.82 \times 10^{-5}$	±0.004	±0.013	±0.076	±0.073	$\pm 2.10 \times 10^{17}$	$\pm 8.32 \times 10^{16}$	±0.008	±0.004
160	5.16×10^{-4}	2.76×10^{-4}	0.78	2.41	4.07	8.62	4.76×10^{17}	1.80×10^{17}	0.67	1.71
	$\pm 5.00 \times 10^{-5}$	$\pm 5.20 \times 10^{-5}$	±0.001	±0.0064	±0.007	±0.059	$\pm 1.97 \times 10^{17}$	$\pm 5.67 \times 10^{16}$	±0.009	±0.007
180	0.0057	3.86×10^{-4}	0.15	0.87	0.96	6.93	3.88×10^{17}	8.77×10^{16}	0.13	0.69
	$\pm 3.50 \times 10^{-3}$	$\pm 6.26 \times 10^{-5}$	±0.074	±0.14	±0.007	±0.059	$\pm 1.61 \times 10^{17}$	$\pm 4.74 \times 10^{16}$	±0.073	±0.10
200		4.52×10^{-4}		0.41		6.90		2.25×10^{17}		0.39
		$\pm 1.79 \times 10^{-4}$		±0.052		±0.023		$\pm 3.41 \times 10^{16}$		±0.046

real parts of Eq. 8, respectively, and ω is the laser modulation angular frequency. Table 1 summarizes the best-fitted parameters using the PCR phase channel alone, because PCR amplitude channel exhibits higher experimental standard deviations due to reflection and transmission. Therefore, the following discussion is based on best-fits to the phase channel because of its better measurement precision. The variances of the best-fitted parameters shown in Table 1 were from 20 computational best-fitted results of each parameter, and the small values indicate high fitting repeatability and uniqueness. Although multiple parameters were extracted through one signal channel (phase fitting), the statistical case for parameter uniqueness was strengthened through the use of 31 frequency points.

Due to the reduced exciton–phonon interactions at low temperatures and a concomitant increase in the radiative emission rate accomplished by the decrease in the non-radiative decay rate when radiative lifetime becomes rate-limiting, the total exciton lifetime τ_2 exhibits an inverse relation with temperature for PbS-EDT/TBAI thin films. In addition, the relative longer exciton lifetimes of PbS-EDT are attributed to the much lower trap-state density N_{T} as shown in Table 1. Exchange ligands, including TBAI and EDT, can effectively passivate QD surface trap sites to increase the exciton lifetime [14]. N_{T} is not a temperature-dependent property and is fitted to be on the order of $10^{17}\mathrm{cm}^{-3}$ for both samples, which is consistent with the results of 1×10^{17} to $2 \times 10^{17}\mathrm{cm}^{-3}$ for PbS-EDT as reported by Carey et al. [15]. Furthermore, due to the multiphonon-assisted hopping mechanisms, lower carrier mobility [16,17] and lower hopping diffusivity D_{h} at low temperatures are expected. The best-fitted values of $D_{\mathrm{h}}(T)$ are similar to the results as reported between 0.003 cm^2/s and 0.012 cm^2/s for PbS CQDs [18]. It is found that PbS-TBAI has relative higher diffusivity when compared with PbS-EDT, indicating a much better photovoltaic material of PbS-TBAI than PbS-EDT. In addition, the higher D_{h} values of PbS-TBAI are agreed with shorter detrapping lifetime τ_i, Table 1. In specific,τ_i of PbS-EDT decreases from 24 μs to 6.9 μs when temperature increases from 100 K to 200 K due to the increased thermal energy responsible for exciton detrapping. PbS-TBAI thin films have a lower τ_i and exhibit a temperature independence behavior. The shorter the exciton residence time in PbS-TBAI trap states, the higher the hopping probability between dots; therefore, higher D_{h} values should be expected. Moreover, the longer PbS-EDT detrapping time is possibly the effect of higher confinement energy when CQDs are surrounded by an insulating EDT ligand matrix [19]. As depicted in Fig. 1f, PCR-phase temperature scans of a PbS-TBAI thin film, the trough shifting to higher temperatures with increased modulation frequency is an indicative of thermal emission from a single trap state. The emission rate acts in resonance with the modulation frequency (deep-level photothermal spectroscopy [6]). In comparison, Fig. 1g shows that the PbS-EDT with lower trap density also exhibited trapping evidence with more peaks/troughs observed when the excitation modulation laser frequency was increased from 1 kHz to 100 kHz. However, instead of exhibiting one dominant trough as shown in Fig. 1f, the multi-trough feature indicates multiple sub-bandgap shallow trap levels in this material. The activation energy of the trap states can be calculated through Arrhenius-plot fitting of the thermal emission rate, e_n [6], as shown in Fig. 1h. e_n is assumed to have an

activation energy E_a and is a Boltzmann function of temperature T [6]:

$$e_n = \gamma_n \sigma_n \exp\left(-\frac{E_a}{kT}\right) \tag{9}$$

where γ_n is a material constant and σ_n is the capture cross section. At each trough, $e_n\left(T_{\text{trough}}\right) = 2.869f$, and f is the pulse repetition frequency [20]. Therefore, the calculated activation energy of PbS-TBAI is about 110 meV, which is close to values reported by Bozyigit et al. [21] for PbS CQDs using thermal admittance spectroscopy (TAS). In contrast, for PbS-EDT, only the 100 kHz temperature scan shows clear separation of peaks, which can be attributed to the fact that the relevant emission rates are too fast for the frequency range $\leq$100 kHz used on these experiments. Therefore, no definitive trap assignments can be made based on the photothermal temperature scans shown in Fig. 1g. Nevertheless, from Fig. 1g, it can be concluded that multiple, shallow, lightly populated trap levels are possible in PbS-EDT, the activation energies of which are hard to demonstrate within the 100 kHz range of these experiments.

5 Conclusions

Coupled with exciton hopping transport theory, PCR, the frequency-domain PL, was used for probing exciton relaxation dynamics and yielded the measurements of five exciton transport parameters of PbS CQD thin films: hopping diffusivity, total and effective exciton lifetimes, exciton detrapping lifetime, and trap-state density. The temperature-dependent hopping diffusivity, also found to be impacted by trap states, shows significant evidence for a phonon-assisted exciton transport mechanism in the studied CQD nanolayers. PCR deep-level photothermal spectra demonstrated that the results were consistent with one dominant trap-state level in PbS-TBAI, whereas multiple trap-state related sub-bandgap shallow energy levels were exhibited in the PbS-EDT sample. The lower trap density of PbS-EDT resulted in longer exciton lifetimes than that of PbS-TBAI.

Acknowledgements The support of the Canada Research Chairs and the Natural Sciences and Engineering Research Council of Canada (NSERC) through a Discovery Grant to AM is gratefully acknowledged.

References

1. E.H. Sargent, Nat. Photonics **6**, 133 (2012)
2. C.H.M. Chuang, P.R. Brown, V. Bulović, M.G. Bawendi, Nat. Mater. **13**, 796–801 (2014)
3. C.H.M. Chuang, A. Maurano, R.E. Brandt, G.W. Hwang, J. Jean, T. Buonassisi, V. Bulovicì, M.G. Bawendi, Nano Lett. **15**, 3286 (2015)
4. A. Mandelis, J. Batista, D. Shaughnessy, Phys. Rev. B **67**, 205208 (2003)
5. J. Batista, A. Mandelis, D. Shaughnessy, Appl. Phys. Lett. **82**, 4077 (2003)
6. J. Xia, A. Mandelis, J. Appl. Phys. **105**, 103712 (2009)
7. J. Wang, A. Mandelis, A. Melnikov, S. Hoogland, E.H. Sargent, J. Phys. Chem. C **117**, 23333 (2013)
8. D. Zhitomirsky, O. Voznyy, S. Hoogland, E.H. Sargent, ACS Nano **7**, 5282 (2013)
9. X. Lan, O. Voznyy, A. Kiani, F.P. García de Arquer, A.S. Abbas, G.H. Kim, M. Liu, Z. Yang, G. Walters, J. Xu, M. Yuan, Adv. Mat. **28**, 299 (2016)

10. M. Liu, F. de Arquer, Y. Li, X. Lan, G.H. Kim, O. Voznyy, L.K. Jagadamma, A.S. Abbas, S. Hoogland, Z. Lu, J.Y. Kim, Adv. Mat. **28**, 4142–4148 (2016)
11. J. Tang, K.W. Kemp, S. Hoogland, K.S. Jeong, H. Liu, L. Levina, M. Furukawa, X. Wang, R. Debnath, D. Cha, K.W. Chou, Nat. Mater. **10**, 765 (2011)
12. A.H. Ip, S.M. Thon, S. Hoogland, O. Voznyy, D. Zhitomirsky, R. Debnath, L. Levina, L.R. Rollny, G.H. Carey, A. Fischer, K.W. Kemp, I.J. Kramer, Z. Ning, A.J. Labelle, K.W. Chou, A. Amassian, E.H. Sargent, Nat. Nanotechnol. **7**, 577 (2012)
13. P.R. Brown, D. Kim, R.R. Lunt, N. Zhao, M.G. Bawendi, J.C. Grossman, V. Bulović, ACS Nano **8**, 5863 (2014)
14. G.W. Hwang, D. Kim, J.M. Cordero, M.W. Wilson, C.H.M. Chuang, J.C. Grossman, M. G. Bawendi Adv. Mat. **27**, 4481 (2015)
15. G.H. Carey, A.L. Abdelhady, Z. Ning, S.M. Thon, O.M. Bakr, E.H. Sargent, Chem. Revs **15**, 12732 (2015)
16. I.H. Chu, M. Radulaski, N. Vukmirovic, H.P. Cheng, L.W. Wang, J. Phys. Chem. C **115**, 21409 (2011)
17. P. Guyot-Sionnest, J. Phys. Chem. Lett. **3**, 1169 (2012)
18. N. Kholmicheva, P. Moroz, E. Bastola, N. Razgoniaeva, J. Bocanegra, M. Shaughnessy, Z. Porach, D. Khon, M. Zamkov, ACS Nano **9**, 2926–2937 (2015)
19. J. Tang, E.H. Sargent, Adv. Mat. **23**, 12 (2011)
20. J. Xia, A. Mandelis, Appl. Phys. Lett. **90**, 062119 (2007)
21. D. Bozyigit, W.M. Lin, N. Yazdani, O. Yarema, V. Wood, Nature Commun. **6**, 6180 (2015)